Carrier injection in nonbonding π states of N-doped graphene by an external electric field

Manaho Matsubara* and Susumu Okada†

Graduate School of Pure and Applied Sciences, University of Tsukuba, Tsukuba, Ibaraki 305-8571, Japan

Using the density functional theory combined with an effective screening medium method, we studied the electronic structure of N-doped graphene under an external electric field. The electronic states near the Fermi level depend on the carrier concentration reflecting their wave function distribution. The electronic states associated with the dangling bond shift upward with increasing electron concentration, following the upward shift of the Fermi level. The electronic states associated with nonbonding π states almost retain their energy upon hole/electron doping by the external electric field.

1. Introduction

Ever since the discovery of graphene, it has been maintaining a premier position not only in the field of nanoscale sciences but also in the field of nanotechnology owing to its unique structural and electronic properties. A hexagonal covalent network of sp^2 C atoms with atom thickness leads to a pair of linear dispersion bands at the Fermi level, enabling us to acquire a two-dimensional electron gas with vanishing effective mass, which underlies the unusual quantum Hall effect,[1,2] and a remarkable carrier mobility of up to 200,000 $cm^2V^{-1}s^{-1}$.[3–5] The characteristic electronic structures of graphene can be modulated by forming hybrid structures with foreign materials, such as atomic/topological defects,[6–11] atomic/molecular adsorbates,[12,13] insulating substrates,[14–16] and other layered materials.[17–19] These external perturbations make graphene a constituent material of functional devices with respect to the electronic structure modulations near the Fermi level, such as the band gap formation and emergence of nonbonding π states around the structural modifications. For the applications of graphene hybrids in real devices, Fermi level tuning is mandatory for controlling their functionality and advancing their efficiency. The electric field further increases the degree of freedom to control the electronic properties of graphene hybrids; bilayer graphene

*E-mail: mmatsubara@comas.frsc.tsukuba.ac.jp
†E-mail: sokada@comas.frsc.tsukuba.ac.jp

is a semiconductor with the direct gap under the electric field normal to the layer.[20–25] The Fermi level is pinned at the energy corresponding to the electronic states of the charge impurity adsorbed on graphene or the dangling bond states in graphene.[24,25] The findings indicate that the electronic properties of graphene hybrids depend on their detailed structure and electric field.

N-doped graphene is one of the representative hybrids exhibiting unusual electronic properties that are applicable to electronic and catalytic devices.[26–36] In such devices, to tailor device properties, it is important to precisely tune the Fermi level by an external electric field. However, the microscopic mechanism of the Fermi level tuning of the N-doped graphene in terms of the external electric field is insufficient for advancing device efficiency. Thus, in this work, we aim to investigate the electronic structure of N-doped graphene under an external electric field with respect to the arrangements of N atoms in a graphene network, using the density functional theory combined with the effective screening medium method. Our calculations show that the electronic states near the Fermi level are sensitive to carrier injection by the external electric field. The electronic states associated with the dangling bond shift upward and downward upon electron and hole injections, respectively, following the Fermi level shift caused by the carrier injection in N-doped graphene. In contrast, the electronic states associated with nonbonding π states almost retain their energy upon carrier injection by the external electric field. The results indicate that the band-filling of the nonbonding π states of N-doped graphene is controllable by adjusting the external electric field.

2. Calculation methods and structural model

All calculations were performed using the density functional theory (DFT)[37,38] with the STATE package.[39] To express the exchange correlation potential among the interacting electrons, local density approximation was applied with the Perdew-Wang functional form fitting to the quantum Monte Carlo results on a homogeneous electron gas.[40] We used ultrasoft pseudopotentials generated by the Vanderbilt scheme to describe the interaction between nuclei and electrons.[41] The valence wave functions and charge density were expanded in terms of the plane-wave basis set with cutoff energies of 25 and 225 Ry, respectively. Brillouin-zone integration was performed with the Γ-centered $4\times4\times1$ uniform $\boldsymbol{k}$-mesh for self-consistent electronic structure calculations for N-doped graphene with 4×4 lateral periodicity, which corresponds to the $16\times16\times1$ $\boldsymbol{k}$-mesh in a primitive 1×1 cell of a pristine graphene, resulting in the sufficient convergence of the

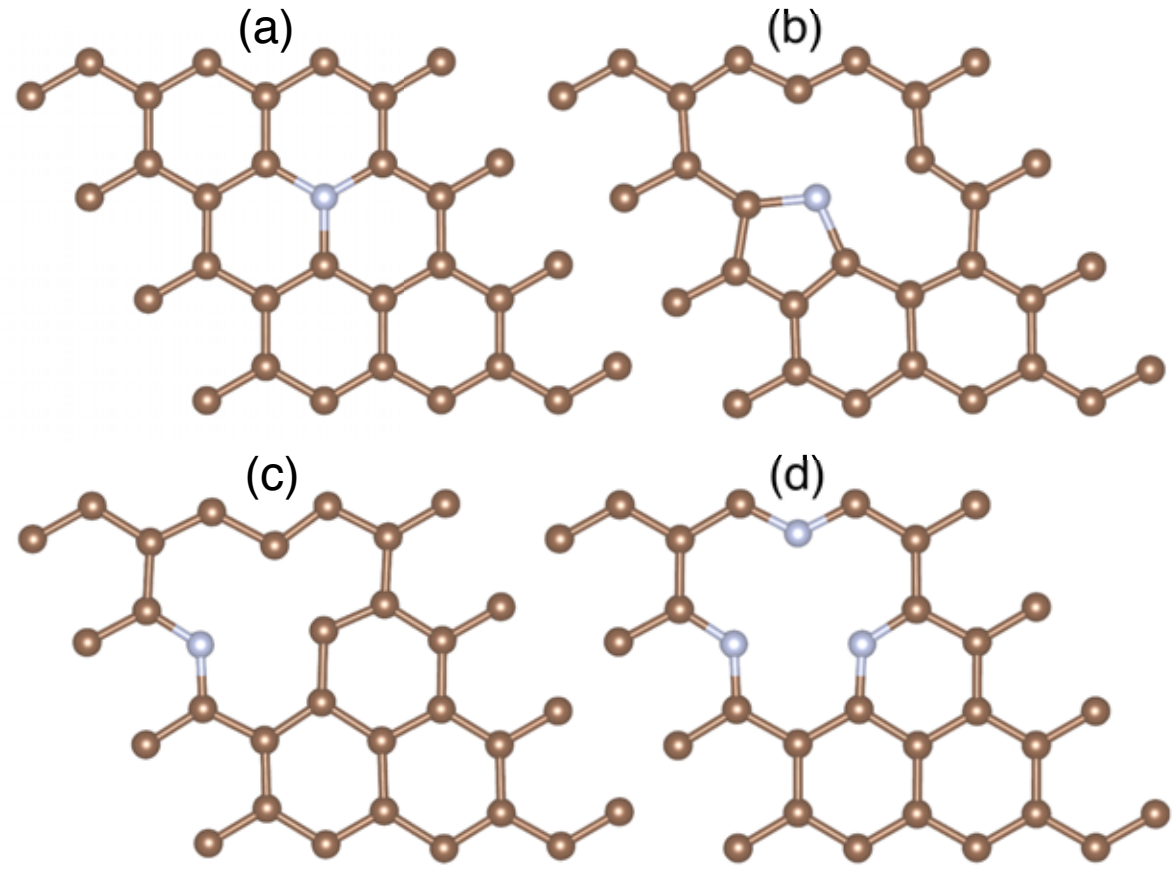

Fig. 1. (Color online) Optimized geometries of N-doped graphene with (a) graphitic, (b) pyrrolic, (c) pylidinic (pyridinic1), and (d) multiple pyridinic (pyridinic3) structures. The brown and purple circles denote C and N atoms, respectively.

geometric and electronic structures. All atoms were fully optimized until the remaining force acting on each atom was less than 0.005 Ry/Å under a fixed lateral lattice constant of 9.83 Å corresponding to the experimental value of a 4×4 lateral cell of graphene.

In the present work, we consider four representative N-doped graphene structures. Figure 1(a) shows the optimized geometry of the N-doped graphene with the graphitic structure in which the N atom is substitutionally implanted in the graphitic network retaining its hexagonal network. Figure 1(b) shows the optimized geometry of N-doped graphene with the pyrrolic structure. For the N-doped graphene with the pyridine structure, we consider two different structures that contain one and three N atoms at the edge of a monatomic vacancy [Figs. 1(c) and 1(d)]. In all these structures, N atoms are doped in the graphene network per 4×4 lateral periodicity. Under the lateral supercell, the N and C atoms retain their planar structure after structural optimization. To investigate the electronic properties of N-doped graphene under electron and hole injections,

we adopted the effective screening medium (ESM) method to solve Poisson's equation under a boundary condition in which a planar metal electrode and half-infinite vacuum are situated at two cell boundaries parallel to the graphene layer.[42] Electrons and holes were injected by the planar gate electrode situated at the upper cell boundary with a vacuum spacing of 4.0 Å to the N-doped graphene layer mimicking the graphene field effect transistor (FET) with a top gate electrode. The electrode was simulated by an effective screening medium with an infinite relative permittivity. During the calculations under a finite electric field, the atomic structure of the N-doped graphene was fixed as the optimized structure obtained under the zero electric field.

3. Results and discussion

Figure 2 shows the electronic energy bands of N-doped graphene under a zero electric field. N-doped graphene does not possess the Dirac cone but a finite energy gap in their π electron state irrespective of the defect species. The electronic structures of N-doped graphene near the Fermi level are sensitive to the defect species. For graphitic N-doped graphene, the Fermi level crosses the dispersive state labeled β. This state exhibits the nonbonding nature of the π states of graphene localized around the N atomic site together with the antibonding nature of N-C bonds. This state may endow N-doped graphene with a graphitic structure with catalytic activity by the precise tuning of the Fermi level because of its nonbonding nature. For the remaining N-doped graphene structures, pyrrolic and pyridinic graphenes possess two or three less dispersive bands near the Fermi level, which intersect dispersive bands derived from graphene π states. The less dispersive bands are associated with dangling bond states at the defects, e.g., the γ and β states for pyrrolic graphene, the γ state for pyridinic graphene (N-pyridinic), and the β state for pyridinic graphene (N3-pyridinic). In addition to the dangling bond states, the nonbonding state forms a less dispersive band near the Fermi level for pyridinic graphene, in which the state also possesses the antibonding nature at the border between N and C atoms.

Figure 3 shows the electronic energy band of N-doped graphene under electron and hole doping. The electronic band structure strongly depends on the geometric structure and carrier species. The electronic energy band exhibits the ridged band feature under the electron and hole doping of graphitic N-doped graphene [Fig. 3(a)]. In contrast, the electronic structures of the remaining three N-doped graphene structures do not exhibit the ridged band nature. Several less dispersive states shift upward and downward upon

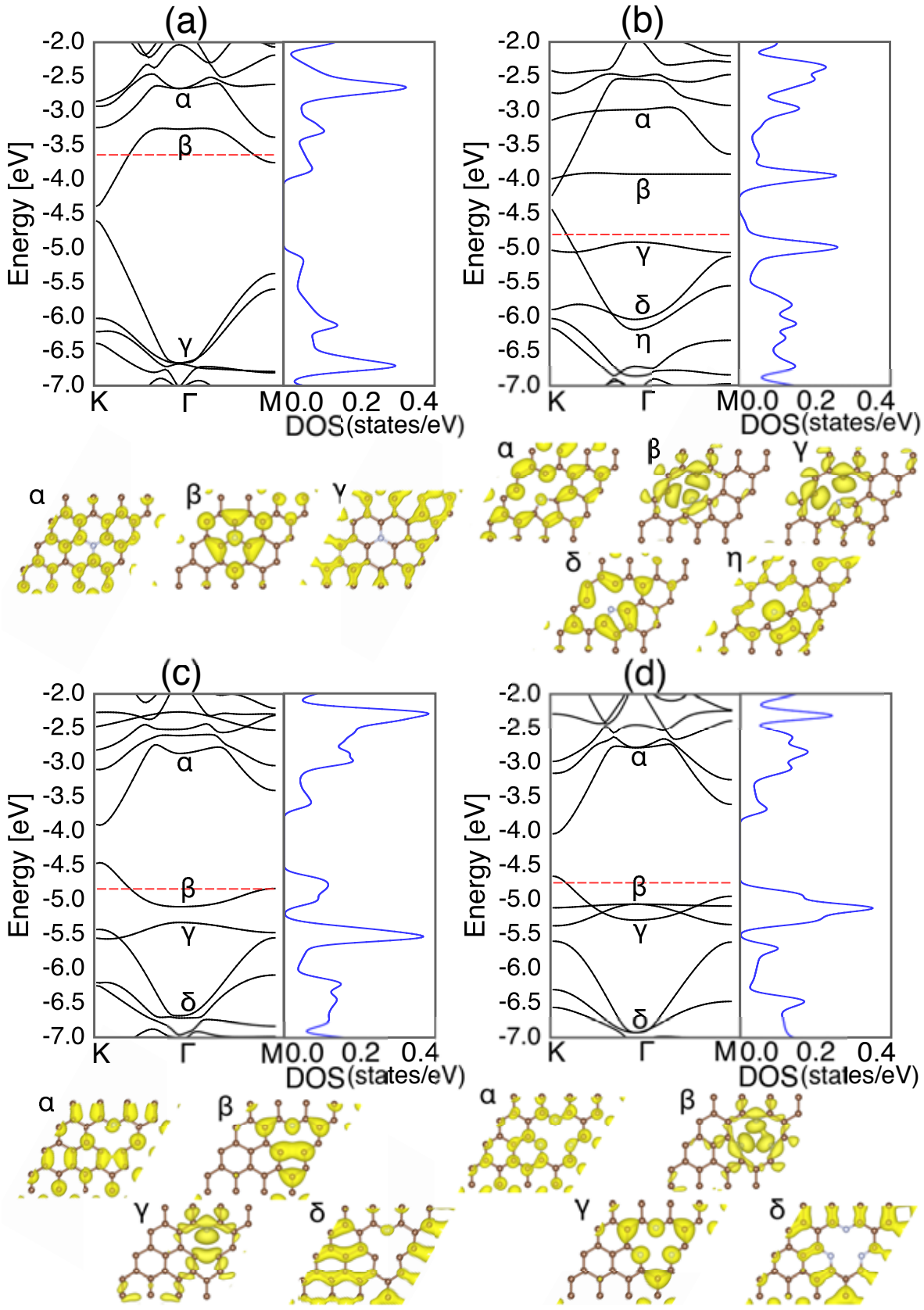

Fig. 2. (Color online) Electronic structure, density of states, and isosurfaces of squared wave function near the Fermi level of N-doped graphene with (a) graphitic, (b) pyrrolic, (c) pyridinic1, and (d) pyridinic3 structures without the external electric field. Labels assigned to wave function correspond to those in the electronic structure. The horizontal dashed line denotes the Fermi level.

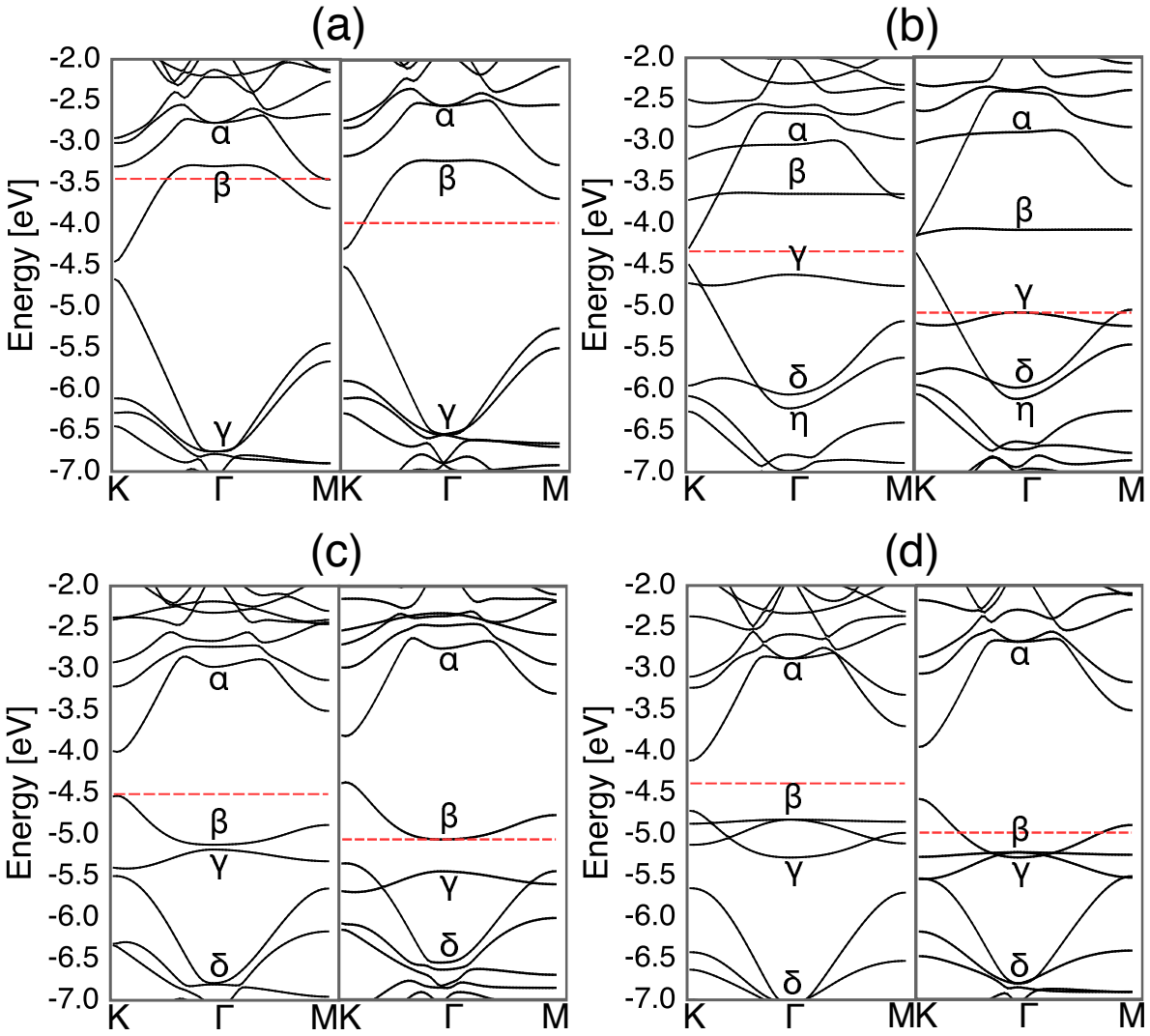

Fig. 3. (Color online) Electronic structures of N-doped graphene with (a) graphitic, (b) pyrrolic, (c) pyridinic1, and (d) pyridinic3 structures with excess carriers of 0.7 e and 0.7 h injected by the counter electrode. In each figure, the left and right panels show the electronic structures under the electron and hole doping, respectively. The red dotted lines denote the Fermi level.

electron and hole doping, respectively. The two flat band states labelled β and γ exhibit downward and upward shifts caused by the hole and electron injections for pyrrolic N-doped graphene [Fig. 3(b)]: The γ state is located at the band edge of the dispersive π state by the electron doping, while the β state is located at the band edge of the antibonding π state by the hole doping. The γ and β states are sensitive to the carrier species for the N-doped graphene with the pyridinic1 structure [Fig. 3(c)] and the pyridnic3 structure [Fig. 3(d)], respectively. These results indicate that the electronic energy band associated with the dangling bond states is sensitive to carrier injection.

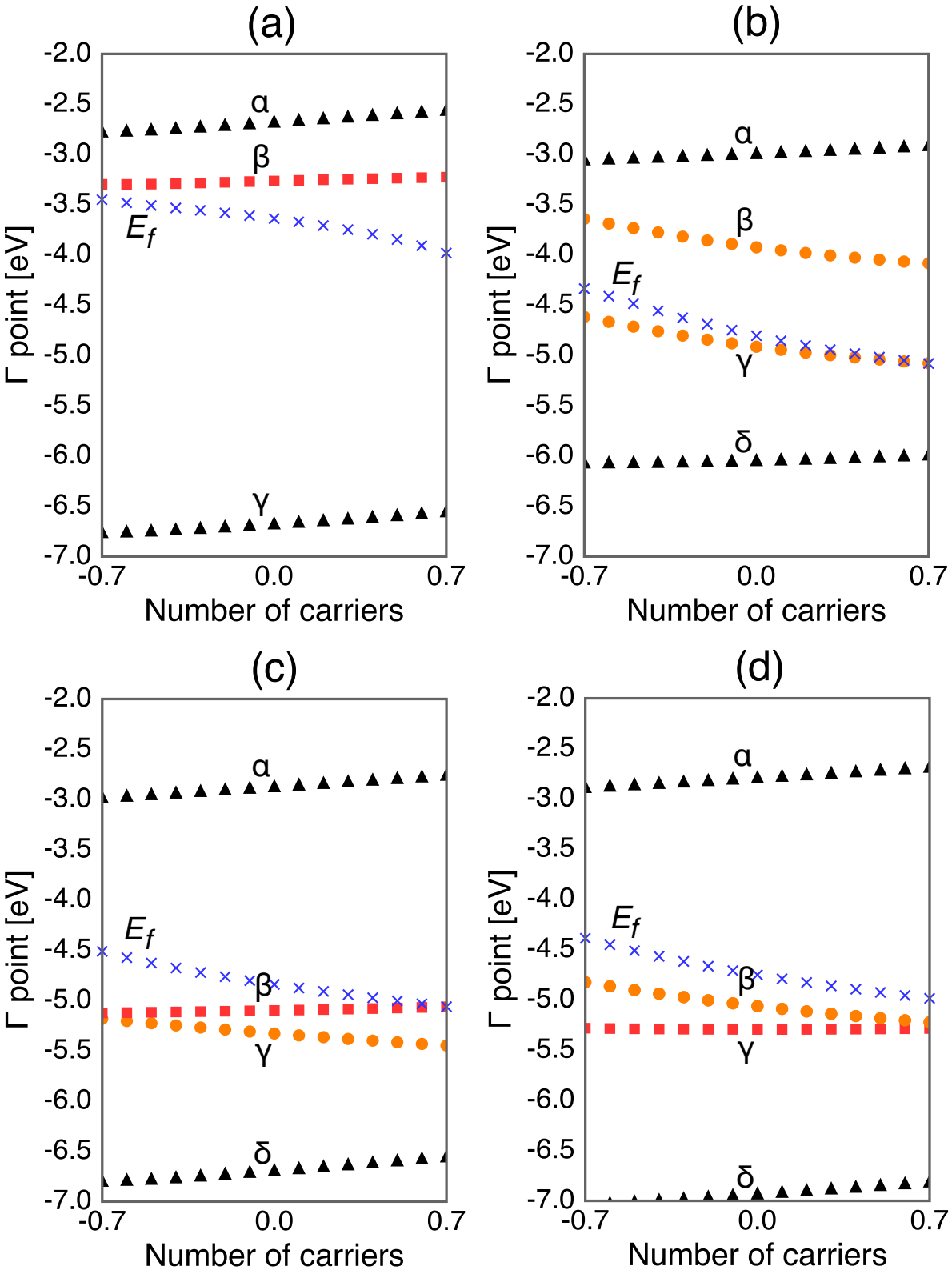

Fig. 4. (Color online) Fermi level energy and eigenvalues of the electronic states near the Fermi level of N-doped graphene with (a) graphitic, (b) pyrrolic, (c) pyridinic1, and (d) pyridinic3 structures as functions of carrier concentration. Labels correspond to those in the electronic structures in Fig. 2. Crosses denote the Fermi level energy.

To investigate the carrier concentration dependence of the electronic energy band, we investigate the Fermi level energy and the eigenvalue of the electronic states near the Fermi level as functions of carrier concentration (Fig. 4). In all cases, the Fermi level monotonically depends on the carrier concentration: The Fermi level shifts upward with increasing number of electrons injected in N-doped graphene in contrast to the graphene adsorbing charged impurities, in which the Fermi level is pinned at the energy associated with the eigenstate of the charged nanoparticles.[25] The results indicate that the gate voltage can be used to tune the Fermi level of N-doped graphene regardless of the N arrangements. The eigenvalue at the Γ point associated with the π electron states is insensitive to the carrier concentration for all N-doped graphene structures. In contrast, the eigenvalue at the Γ point associated with the dangling bond state monotonically increases with increasing electron concentration. Therefore, the electron filling of the nonbonding π electron states is tunable by adjusting the external electric field induced by the gate electrode in FET structures. The filling control of these states enhances or deteriorates the chemical reactivity of N-doped graphene under the FET structure. The upward shift of dangling bond states upon electron injection is ascribed to the large onsite Coulomb's repulsive interaction under electron doping in these states. On the other hand, nonbonding π states exhibit a relatively extended nature compared with the dangling bond state, making the states insensitive to electron doping.

The distribution of the accumulated carriers in N-doped graphene under the external electric field is worth investigating. Figure 5 shows the isosurfaces of the accumulated carriers in the N-doped graphene with 0.7 e and 0.7 h under the external electric field. Since the Fermi level crosses the dispersive bands associated with the nonbonding states induced by N doping, injected carriers are primarily accommodated in the nonbonding π states under the finite external electric field induced by the gate electrode. Furthermore, for the N-doped graphene with the pyrrolic and pyridinic structures, the dangling bond states are also located near the Fermi level. Thus, these states also contribute to carrier injection. For the N-doped graphene with the graphitic structure, the injected carriers have the nonbonding π electron nature as the states that cross the Fermi level for both electron and hole doping [Fig. 5(a)]. For the N-doped graphene with the pyrrolic and pyridinic structures, the electrons and holes are accommodated in not only the nonbonding π electron states around the N atoms but also the dangling bond states just below the Fermi level [Figs. 5(b)-5(d)]. Because of the upward and downward shifts of the dangling bond states upon electron and hole injections, respectively, these states

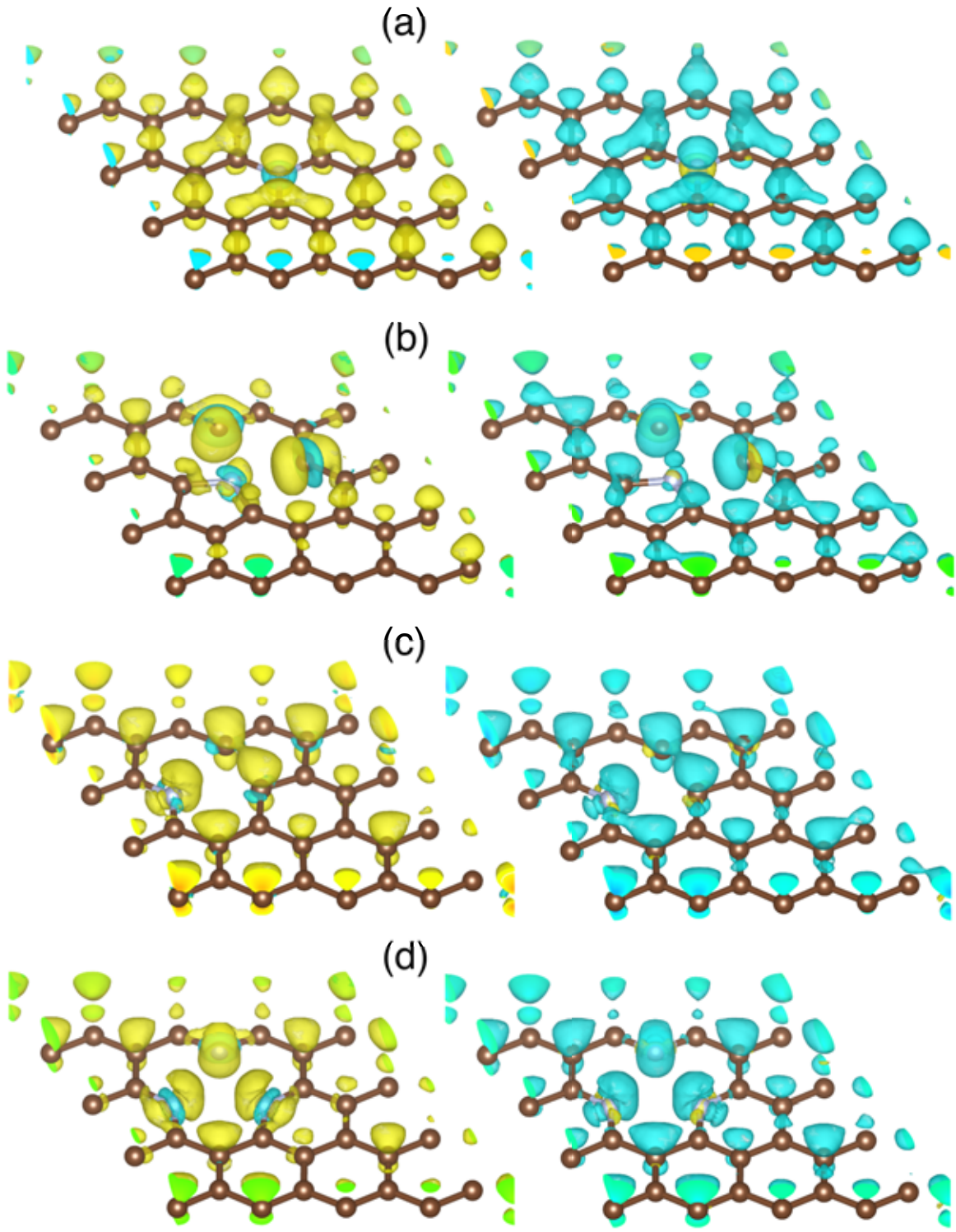

Fig. 5. (Color online) Isosurfaces of accumulated carrier in N-doped graphene with (a) graphitic, (b) pyrrolic, (c) pyridinic1, and (d) pyridinic3 structures. In each figure, the left and right panels show the isosurfaces under 0.7e and 0.7h doping, respectively. The yellow and cyan surfaces denote the regions of electron accumulation and depression, respectively.

symmetrically contribute to the carrier injection in N-doped graphene with dangling bond states. Furthermore, the distribution of the accumulated carriers corroborates the physical mechanism that N-doped graphene with the pyrrolic and pyridinic structures does not exhibit the ridged band nature owing to the energy shift of the dangling bond states depending on the carrier concentration.

Figure 6 shows the contour plots of electrostatic potential upon the electron and hole injections in N-doped graphene. Because of carrier concentration around the N atom and its adjacent C atoms, the electrostatic potential is spatially modulated within the graphene layer. For the electron doping, the potential near the N atomic site is higher than that near the C atomic site owing to the electron accumulation. On the other hand, the potential around the N atomic site is lower than that around the C atomic site for the hole doping, owing to the electron depression. Since the distribution of accumulated carriers is approximately symmetric for electron and hole doping, the electrostatic potential also exhibits a symmetric feature upon carrier doping. The spatially modulated electrostatic potential implies that carrier injection can control the chemical reactivity of molecules around N atomic sites: Molecular adsorptions to N-doped graphene may strongly depend on the molecular orientation and carrier concentration, so that the selective adsorption of molecules possessing a dipole moment, such as CO and NO_x, controls the catalytic reactivity of N-doped graphene in a FET structure.

4. Conclusions

We have studied the electronic structure of N-doped graphene under an external electric field to investigate the possibilities of electron-filling control and the Fermi level tuning by the field. Our calculations showed that the electronic states near the Fermi level depend on the carrier concentration injected by the external electric field. The electronic states associated with the dangling bond shift upward with increasing number of electrons injected by the electrode. In contrast, electronic states associated with nonbonding π states almost retain their energy upon carrier injection by the external electric field. We also demonstrated that the Fermi level monotonically increases with increasing electron concentration. The results indicate that the band filling of the nonbonding π states of N-doped graphene is controllable by adjusting the external electric field. The upward shift of dangling bond states following the Fermi level shift is ascribed to the large Coulomb repulsive interaction for the injected electron in the states.

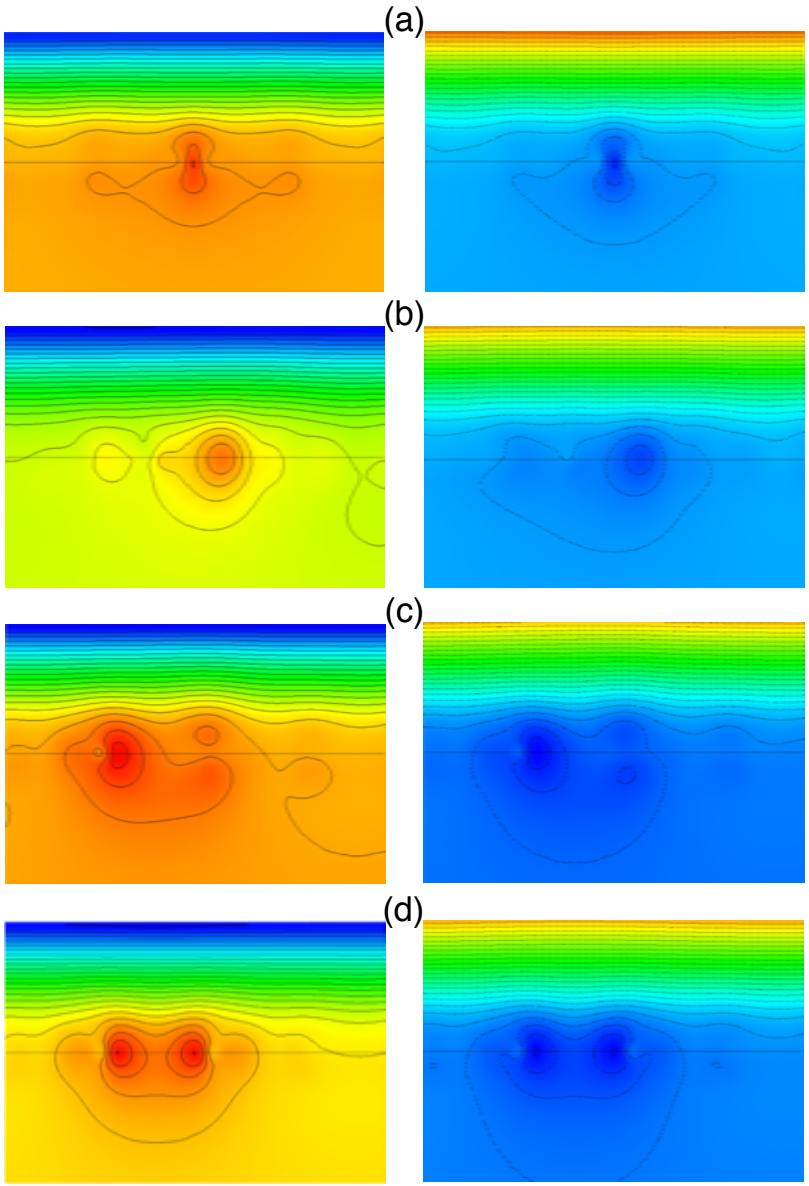

Fig. 6. (Color online) Contour plots of the electrostatic potential upon electron and hole injections in N-doped graphene with (a) graphitic, (b) pyrrolic, (c) pyridinic1, and (d) pyridinic3 structures. In each figure, the left and right panels show the contour plots under 0.7e and 0.7h doping, respectively. The vertical dotted lines denote the graphene layer. The counter electrode is located at the top of each panel. Red and blue denote the area corresponding to the high and low electrostatic potentials, respectively. Note that the steep potential variation at the top of each figure corresponds to the electrode region.

Acknowledgments

This work was supported by CREST, from the Japan Science and Technology Agency, JSPS KAKENHI Grant Numbers JP25246010, JP16H00898, and JP16H06331 from the Japan Society for the Promotion of Science, and the Joint Research Program on

Emission Energy Research, Institute of Advanced Energy, Kyoto University. Part of the calculations was performed on an NEC SX-Ace at the Cybermedia Center at Osaka University and on an SGI ICE XA/UV at the Institute of Solid State Physics, The University of Tokyo.

References

1) K. S. Novoselov, A. K. Geim, S. V. Morozov, D. Jiang, M. I. Katsnelson, I. V. Grigorieva, S. V. Dubonos, and A. A. Firsov, Nature **438**, 197 (2005).
2) Y. Zhang, Y.-W. Tan, H. L. Stormer, and P. Kim, Nature **438**, 201 (2005).
3) K. I. Bolotin, K. J. Sikes, Z. Jiang, M. Klima, G. Fudenberg, J. Hone, P. Kim, and H. L. Stormer, Solid State Commun. **146**, 351 (2008).
4) J. B. Oostinga, H. B. Heersche, X. Liu, A. F. Morpurgo, and L. M. K. Vandersypen, Nat. Mater. **7**, 151 (2007).
5) Y. Zhang, T. Tang, C. Girit, Z. Hao, M. C. Martin, A. Zettl, M. F. Crommie, Y. R. Shen, and F. Wang, Nature **459**, 820 (2009).
6) Y. Ma, P. O. Lehtinen, A. S. Foster, and R. M. Nieminen, New J. Phys. **6**, 68 (2004).
7) H. Amara, S. Latil, V. Meunier, Ph. Lambin, and J.-C. Charlier, Phys. Rev. B **76**, 115423 (2007).
8) M. M. Ugeda, I. Brihuega, F. Hiebel, P, Mallent, J.-Y. Veuillen, J. M. G.-Rodriguez, and F. Yndurain, Phys. Rev. B **85**, 121402(R) (2012).
9) M. Dvorak, W. Oswald, and Z. Wu, Sci. Rep. **3**, 2289 (2013).
10) P. Koskinen, S. Malola, and H. Hakkinen, Phys. Rev. Lett. **101**, 115502 (2008).
11) S. Okada, T. Kawai, and K. Nakada, J. Phys. Soc. Jpn. **80**, 013709 (2011).
12) N. Igami, K. Nakada, and S. Okada, Synth. Met. **121**, 1233(2001).
13) R. Balog, B. Jorgensen, L. Nilsson, M. Andersen, E. Rienks, M. Bianchi, M. Fanetti, E. Laegsgaard, A. Baraldi, S. Lizzit, Z. Sljivancanin, F. Besenbacher, B. Hammer, T. G. Pedersen, P. Hofmann, and L. Hornekaer, Nat. Mater. **9**, 315 (2010).
14) S. Y. Zhou, G.-H. Gweon, A. V. Fedorov, P. N. First, W. A. de Heer, D.-H. Lee, F. Guinea, A. H. C. Neto, and A. Lanzara, Nat. Mater. **6**, 770 (2007).
15) N. T. Cuong, M. Otani, and S. Okada, Phys. Rev. Lett. **106**, 106801 (2011).
16) K. Kamiya, N. Umezawa, and S. Okada, Phys. Rev. B **83**, 153413 (2011).
17) A. Mattausch and O. Pankratov, Phys. Rev. Lett. **99**, 076802 (2007).
18) M. Koshino and T. Ando, Phys. Rev. B **76**, 085425 (2007).
19) M. Otani, M. Koshino, Y. Takagi, and S. Okada, Phys. Rev. B **81**, 161403(R) (2010).
20) E. McCann, Phys Rev. B **74**, 161403 (2006).

21) E. V. Castro, K. S. Novoselov, S. V. Morozov, N. M. R. Peres, J. M. B. Lopes dos Santos, J. Nilsson, F. Guinea, A. K. Geim, and A. H. Castro Neto, Phys. Rev. Lett. **99**, 216802 (2007).
22) M. Otani and S. Okada, J. Phys. Soc. Jpn. **79**, 073701 (2010).
23) S. Konabe and S. Okada, J. Phys. Soc. Jpn. **81**, 113702 (2012).
24) K. Kishimoto and S. Okada, Appl. Phys. Lett. **110**, 011601 (2017).
25) M. Matsubara and S. Okada, Appl. Phys. Express **10**, 025101 (2017).
26) D. Wei, Y. Liu, Y. Wang, H. Zhang, L. Huang, and G. Yu, Nano Lett. **9**, 1752 (2009).
27) X. Wang, X. Li, L. Zhang, Y. Yoon, P. K. Weber, H. Wang, J. Guo, and H. Dai, Science **324**, 768 (2009).
28) D. Usachov, O. Vilkov, A. Gruneis, D. Haberer, A. Fedorov, V. K. Adamchuk, A. B. Preobrajenski, P. Dudin, A. Barinov, M. Oehzelt, C. Laubschat, and D. V. Vyalikh, Nano Lett. **11**, 5401 (2011).
29) G. Imamura and K. Saiki, J. Phys. Chem. C **115**, 10000 (2011).
30) Z. Jin, J. Yao, C. Kittrell, and M. Tour, ACS Nano **5**, 4112 (2011).
31) Y. Fujimoto and S. Saito, Phys. Rev. B **84**, 245446 (2011).
32) Z. Hou, Z. Wang, T. Ikeda, K. Terakura, M. Oshima, M. Kakimoto, and S. Miyata, Phys. Rev. B **85**, 165439 (2012).
33) T. Susi, J. Kotakoski, R. Arenal, S. Kurasch, H. Jiang, V. Skakalova, O. Stephan, A. V. Krasheninnikov, E. I. Kauppinen, U. Kaiser, and J. C. Meyer, ACS Nano **6**, 8837 (2012).
34) Y. Fujimoto and S. Saito, Appl. Phys. Lett. **115**, 153701 (2014).
35) T. Kondo, T. Suzuki, and J. Nakamura, J. Phys. Chem. Lett. **2**, 577 (2011).
36) T. Kondo, S. Casolo, T. Suzuki, T. Shikano, M. Sakurai, Y. Harada, M. Saito, M. Oshima, M. I. Trioni, G. F. Tantardini, and J. Nakamura, Phys. Rev. B **86**, 035436 (2012)
37) P. Hohenberg and W. Kohn, Phys. Rev. **136**, B864 (1964).
38) W. Kohn and L. J. Sham, Phys. Rev. **140**, A1144 (1965).
39) Y. Morikawa, K. Iwata, and K. Terakura, Appl. Surf. Sci. **169-170**, 11 (2001).
40) J. P. Perdew and Y. Wang, Phys. Rev. B **45**, 13244 (1992).
41) D. Vanderbilt, Phys. Rev. B **41**, 7892 (1990).
42) M. Otani and O. Sugino, Phys. Rev. B **73**, 115407 (2006).